Hindawi
International Journal of Energy Research
Volume 2024, Article ID 5928926, 13 pages
https://doi.org/10.1155/2024/5928926

Research Article

Analysis of Confined Jet Impingement in Converging Annular Microchannel Heat Sinks

Mohsen Mashhadi Keshtiban, Mohammad Zabetian Targhi, and Mohammad Mahdi Heyhat

Department of Mechanical Engineering, Tarbiat Modares University, Tehran, Iran

Correspondence should be addressed to Mohammad Zabetian Targhi; zabetian@modares.ac.ir

Received 12 October 2023; Revised 3 February 2024; Accepted 22 February 2024; Published 27 March 2024

Academic Editor: Hamza Faraji

Jet impingement cooling is deemed an excellent choice for the thermal management of high-power electronics. However, high-pressure drop penalties and low local heat transfer coefficients in regions far from the jet zone are its drawbacks. Although it is reported that recirculation areas appear because of the entrainment, the effects of recirculation size on thermal behavior are not understood well enough. Here, jet impingement heat sinks with converging annular channels are employed in a numerical investigation to minimize the adverse cooling effects associated with an impinging jet in a microchannel. The realizable $k-\varepsilon$ turbulent model is used for modeling thermal and turbulent flow fields (Re = 5,000 to 25,000). It was found that the different flow recirculation zones in small scales are responsible for the enhanced heat transfer rate. While the thermal performance of a converging wall jet impingement heat sink is higher than its flat wall counterpart at low Re numbers, the thermal performance results are in favor of the flat wall jet impingement heat sink at high Re numbers. The flow recirculation area shrinks in converging channels at high Re numbers, thereby deteriorating the thermal performance of the converging channel compared with a flat wall jet heat sink. Also, it was found that employing steeper converging channels shrinks the flow recirculation region, resulting in up to 59% lower pressure drops at Re = 25,000. The present study examines the role of flow recirculation at different Re numbers on the thermohydraulic performance of jet impingement converging annular heat sinks.

1. Introduction

The microelectronics industry has been proliferating during the last few decades. This rise is driven by advances in microelectronics fabrication and packaging technologies and the desire to improve microelectronics performance through device scaling. Modern systems demand higher power and operating frequencies, which lead to high heat fluxes. At high temperatures, electronic chips fail to deliver their designed functionalities and have a reduced lifetime. Mini and microchannels are designed to overcome these issues while supported by numerical optimization studies [1] and employing different geometrical configurations such as jet impingement [2], pin fins [3, 4], ribs [5], bifurcation plates [6], and porous materials [7, 8].

Many prior single-phase jet impingement investigations have shown higher heat transfer coefficients than parallel flow heat sinks. Electronic cooling [9], gas turbine blade cooling [10], mixing [11], heaters [12], and food processing [13] are a few industrial applications of jet impingement. The impacts of geometrical parameters such as jet configuration, jet array layout, nozzle diameter, jet-to-target distance, nozzle shape, and jet-fin combination [14, 15] have been investigated in past studies with both confined and unconfined configurations [16, 17].

Jet impingement improves the heat transfer rate at the jet center [18]. Particularly, multiple jet inlets assist in maintaining low base temperatures and augment the overall thermal performance of the system [19]. Optimized jet arrays help heat sinks in achieving better performance levels and

dissipate a higher heat flux. Geometric parameters influence the characterization of jet fluid as well. For instance, jet-to-target distance and nozzle diameter may enhance or deteriorate the performance considering the operating conditions [20, 21]. It is also possible to enhance jet impingement by employing extended surfaces such as microfines [22, 23], ribs [24], dimples [25], and porous materials [26, 27]. However, this may lead to more significant pressure drops, so the design of microbarriers should be prioritized first [28–30].

It is reported that the jet entrainment changes the hydrothermal characteristics of the heat sink [31]. Nuntadusit et al. [32] employed a secondary duct for studying the effects of entrainment numerically. They found that mounting an air-augmented duct for modifying jet entrainment can increase the turbulent intensity and flow velocity of the jet before impingement. Guo et al. [33] studied jet development visually using PIV. They reported the presence of recirculation in the jet wall zone and called them minor vortexes, the same as in previous investigations [34]. They showed that the location of the core vortex and decay range vary at different configurations. Although the earlier studies reported the presence of recirculation because of the entrainment, there is no much information about the effects of vortex size on the thermal characteristics.

It has also shown that using a variable cross-sectional channel area might enhance the performance of the heat sinks [35]. Converging and diverging channels are simple types of variable cross-section heat sinks, and their combination with other approaches is available. Hajmohammadi et al. [36] studied the effect of diverging channels on the heat transfer performance of simple and porous channels and found that thermal performance decreases in width-wise diverging and increases for height-wise diverging channels. Duryodhan et al. [37] showed that the converging channels offer higher thermal performances compared to the diverging ones. Yousefi et al. [38] studied laminar jet impingement in a converging channel numerically. They reported more than a 24% improvement in the averaged Nusselt number and a 50% increase in surface friction. However, the above research lacked studying turbulent flows and the associated vortexes in converging channels, and the combination of a confined turbulent jet and converging wall needs to be investigated.

Although the heat transfer performance of the laminar jet impingement has been extensively studied, more investigation on the heat transfer physics of the confined turbulent jet impingement is required on small scales. A turbulent jet flow regime could offer higher heat transfer rates. However, the interaction of a turbulent jet and a microconverging channel is complex and warrants additional studies. Although the presence of vortexes in the wall jet regions is reported, their effects on thermohydraulic characteristics remain inadequately documented, and its impact may vary across different scenarios. This work focuses on the numerical investigation of three-dimensional steady-state turbulent jet liquid flows in radial convergent heat sinks to study the effects of recirculation size in a heat sink. The jet physics at different Re numbers are studied, and the effects of the converging channels on thermohydraulic performance are presented. The radial heat sink is heated at the bottom metallic surface and cooled by an impinging water jet flow. Hydrodynamic and thermal analyses are performed on the converging channels at different height ratios (HRs).

2. Computational Model

2.1. Problem Description. The liquid cooling system consists of a confined jet impinging on a radial converging channel. Figure 1 shows a 3D schematic and a cross-sectional view of the heat sink with converging annular channels. As shown, cold fluid enters the heat sink from the central section and impinges the hot bottom surface. Then, the fluid flows in a radial direction and exits from the outer part of the heat sink. The bottom solid medium is considered aluminum. The heat flux is exposed to the heat sink from the bottom horizontal surface. The dimension of the aluminum base is 30 mm in diameter and 1 mm in thickness. The channel height and jet inlet diameter are both 3 mm. These geometrical dimensions are considered based on the liquid cooling of the electronic devices and for investigating the effects of recirculation areas.

2.2. Governing Equations. To study the detail of the jet impingement process, the transport governing equations were solved in both fluid and solid domains. The $k-\varepsilon$ turbulent models were employed in previous studies due to their reasonable accuracy and lower computational costs compared to the other turbulence models [39–41]. The realizable k-epsilon model offers more precise predictions of the spreading rate of planar and round jets. Additionally, it demonstrates improved performance in scenarios involving boundary layers under significant adverse pressure gradients, recirculation, and separation [42, 43]. As a result, the realizable $k-\varepsilon$ turbulent model is used for thermal and turbulent flow field modeling.

Continuity and momentum equations are as follows:

$$\frac{\partial u_i}{\partial x_j} = 0, \tag{1}$$

$$u_j \frac{\partial u_i}{\partial x_j} = -\frac{\partial P}{\partial x_i} + \vartheta \frac{\partial^2 u_i}{\partial x_j \partial x_j}. \tag{2}$$

Energy equations for fluid and solid are as follows:

$$\frac{\partial (u_i T)}{\partial x_i} = k_f \frac{\partial^2 T}{\partial x_i \partial x_i}, \tag{3}$$

$$k_s \frac{\partial^2 T}{\partial x_i \partial x_i} = 0. \tag{4}$$

Turbulent equations for modeling are

$$\frac{\partial}{\partial x_j}\left(\rho K_e u_j\right) = \frac{\partial}{\partial x_j}\left[\left(\mu + \frac{\mu_t}{\sigma_{K_e}}\right)\frac{\partial K_e}{\partial x_j}\right] + G_k + G_b + \rho\varepsilon - Y_m + S_{K_e}, \tag{5}$$

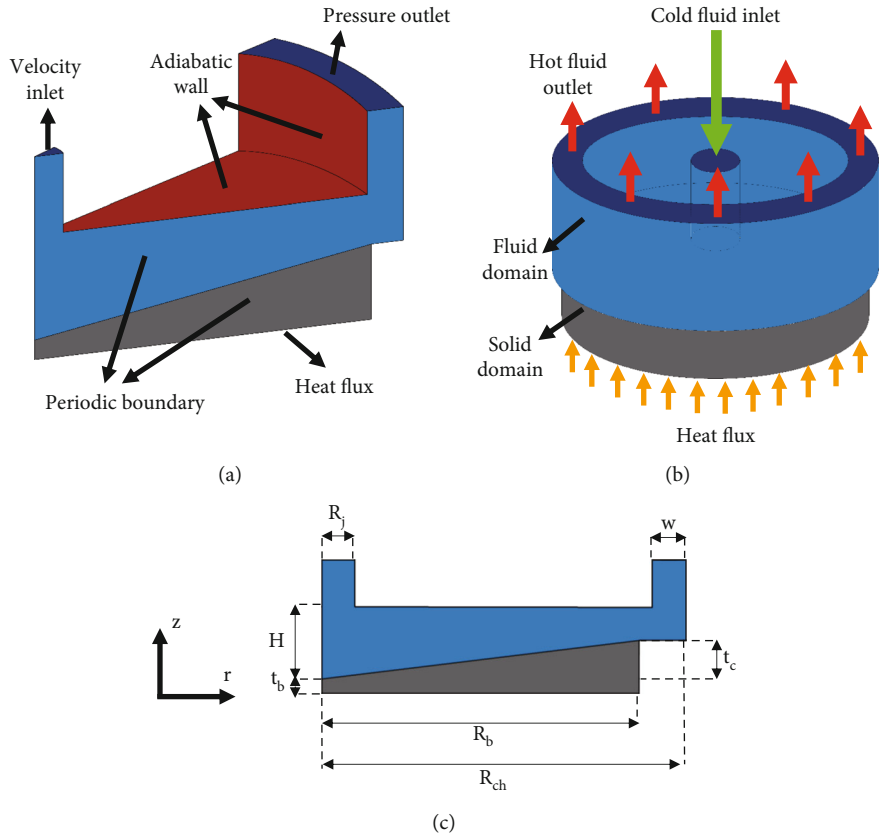

Figure 1: (a) A 22.5° slice of the heat sink used as the computational domain, (b) a 3D schematic view, and (c) a cross-sectional view of the convergent heat sink.

$$\frac{\partial}{\partial x_j}\left(\rho\varepsilon u_j\right) = \frac{\partial}{\partial x_j}\left[\left(\mu + \frac{\mu_t}{\sigma_{K_e}}\right)\frac{\partial \varepsilon}{\partial x_j}\right] + \rho C_1 S_\varepsilon - \rho C_2 \frac{\varepsilon^2}{K_e + \sqrt{\vartheta\varepsilon}} + C_{1\varepsilon}\frac{\varepsilon}{K_e} C_{3\varepsilon} G_b + S_\varepsilon, \tag{6}$$

$$\mu_t = \rho C_\mu \frac{{K_e}^2}{\varepsilon}, \tag{7}$$

where different source terms in these equations are described in Ref. [44].

The following assumptions are considered:

(i) Steady-state flow and heat transfer mechanisms

(ii) Newtonian and incompressible fluid

(iii) No slip boundary condition at the solid boundaries

(iv) Negligible heat radiation, viscous dissipation, gravitational forces, natural convection, and other body forces

2.3. Numerical Method and Data Reduction. Ansys Fluent was employed to simulate the flow and heat transfer physics of the jet impingement heat sink. The finite volume method, pressure-based solver, and second-order upwind differencing approach were used for energy and momentum equations. The Semi-Implicit Method for Pressure Linked Equation (SIMPLE) technique was used for pressure-velocity coupling and the second-order upwind scheme for the numerical discretization. Scaled residuals of 10^{-6} for momentum and continuity and 10^{-8} for energy equations were considered for convergence. To reduce the computational cost, a 22.5° (1/16) slice of the geometry was simulated, as its results did not show any differences between 45° and 90° slices. The periodic boundary condition was set as presented in Figure 1(a).

Table 1: Geometric parameter values.

Parameter	Values	Unit
k_s	205	W/(m·K)
k_f	0.6	W/(m·K)
μ	0.001	Pa·s
R_j	1.5	mm
R_b	15	mm
R_{ch}	17.5	mm
w	2	mm
H	3	mm
t_b	1	mm
HR	0.25, 0.5, 0.75, 1	—

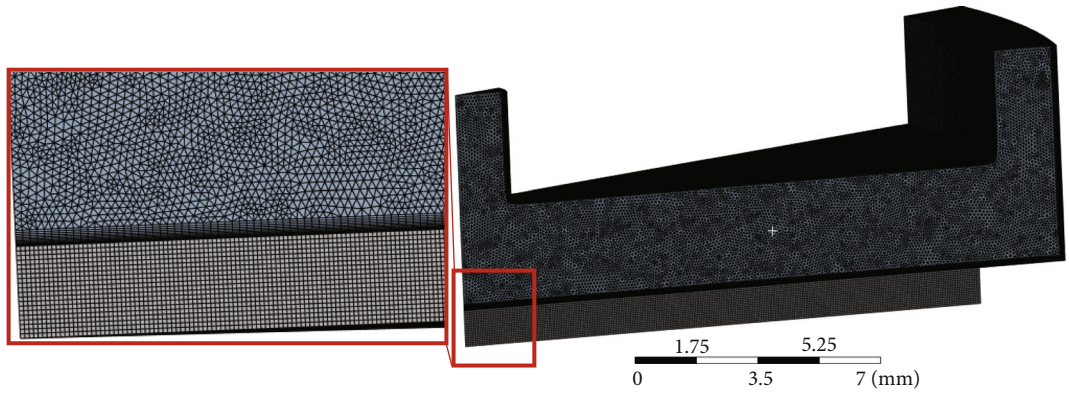

Figure 2: A sample discretized meshed domain.

Uniform velocity and temperature boundary conditions with a turbulence intensity of 5% and a turbulence viscosity ratio of 10 were considered at the inlet. Also, constant pressure and heat flux boundary conditions were considered at the outlet and the bottom surface, respectively. All other solid boundaries were specified to be adiabatic. A list of the boundary conditions is summarized below:

At inlet, $U = U_j$, and $T = T_j = 25^{\circ}\text{C}$.

At outlet, $P = P_{\text{out}} = 0$.

At the fluid-solid interface, $u = 0$, $T_f = T_s$, and $k_f(\partial T_f/\partial z) = k_s(\partial T_s/\partial z)$.

At the base wall, $q_w'' = -k_s(\partial T/\partial z) = 40\text{W/cm}^2$.

The average heat transfer coefficient, thermal resistance, and Nu number of the heat sink are calculated as follows:

$$h_{\text{ave}} = \frac{q}{A_{s,f}\left(T_{s,f} - T_f\right)}, \tag{8}$$

$$R = \frac{A_b\left(T_{\text{base}} - T_f\right)}{q}, \tag{9}$$

$$\text{Nu} = \frac{h_{\text{ave}} D_j}{k_f}, \tag{10}$$

where

$$T_f = \frac{T_{f,\text{in}} + T_{f,\text{out}}}{2}, \tag{11}$$

where $T_{s,f}$, T_f, and T_{base} are the average temperature at the fluid-solid interface, the average fluid temperature, and the average temperature of the base wall, respectively.

Also, the Re number is defined considering the inlet jet velocity and diameter as follows:

$$\text{Re}_j = \frac{\rho U_j D_j}{\mu}. \tag{12}$$

Table 2: Average heat transfer coefficient and their percentage differences at different numbers of computational elements.

Number of elements	Average heat transfer coefficient (W/m^2-K)	Percentage difference in average heat transfer coefficient
1,501,684	20,400	21%
2,231,548	21,950	15%
4,321,986	25,825	1.5%
8,854,734	26,212	—

The local heat transfer coefficient is calculated as follows:

$$h_{\text{local}} = \frac{q''_r}{\left(T_r - T_{f,\text{bulk}}\right)}, \tag{13}$$

where T_r and q''_r are the temperature at the fluid-solid interface and heat flux at a given radius. Also, $T_{f,\text{bulk}}$ is defined as the fluid bulk temperature at a given radius and calculated as follows:

$$T_{f,\text{bulk}} = \frac{\int TU.dA}{\int U.dA}. \tag{14}$$

The normalized heat transfer coefficient and pressure drop are defined against the flat parallel-wall heat sink as follows:

$$h^* = \frac{h}{h_0}, \tag{15}$$

$$\Delta P^* = \frac{\Delta P}{\Delta P_0}, \tag{16}$$

where h_0 and ΔP_0 are the average heat transfer coefficient and pressure drop of the flat heat sink.

The pumping power of a heat sink is calculated as

$$\text{Pumping power}\,(W) = \Delta P \times Q, \tag{17}$$

Table 3: A comparison between the experimental and numerical Nu number of Tang et al. [45] and numerically calculated Nu number of present study.

Cone angle	Experimental Nu [45]	Numerical Nu [45]	Numerical Nu (present study)	Deviation from experimental results	Deviation from numerical results
0°	1,238	1,254.6	1,220	1.45%	2.7%
45°	1,347	1,380	1,303	3.24%	5%

where Q is the flow rate. Also, the main important geometrical and computational parameters are listed in Table 1. The converging height ratio (HR) is defined as the ratio of the channel height at the exit to the channel height at the inlet.

$$\mathrm{HR} = \frac{(H - t_c)}{H}. \tag{18}$$

Also, the recirculation length ratio is defined as

$$\mathrm{LR} = \frac{L_v}{R_{\mathrm{ch}}}, \tag{19}$$

where L_v is vortex length in the channel.

2.4. Grid Independence Study and Model Validation. Figure 2 shows a sample discretized meshed domain generated in ANSYS Meshing software. To adequately determine the turbulent boundary layer, a minimum of eleven inflation layers with a $y+ \approx 1$ were maintained in the impingement zone of the fluid domain. Four grid sizes were considered for the mesh independence study, as listed in Table 2. The grid independence study was evaluated based on the average heat transfer coefficient at Re = 25,000. The difference in the average heat transfer coefficients of the heat sinks with 4.3 and 8.8 million meshes is less than 2%. Therefore, a heat sink discretized with 4.3 million meshes was chosen.

Tang et al. [45] investigated the confined jet impingement on a flat surface and 45° cone experimentally and numerically. The Nusselt number of their results is employed for model validation. The average Nu for the numerical approach and experimental data of 0° and 45° cone are presented in Table 3. The experimental and numerical data was presented at jet Re number of 25,000 and heat flux of 80 W/cm^2. As evident, the error between the experimentally measured and numerically calculated Nu numbers is less than 3.3%.

3. Results and Discussion

The thermohydraulic performances of the converging annular channels at height ratios of 0.25, 0.5, 0.75, and 1 were numerically investigated. The coolant Re number varied between 5,000 and 25,000. A careful study of streamlines, velocity profiles, and contours helped clarify important flow and heat transfer features in converging annular channels.

3.1. Effects of Converging Channels on Hydrodynamic Parameters. As can be seen in Figure 3(a), the flow zones in a jet impingement device consist of three distinct regions of the free jet, stagnation, and wall jet. The zone where flow develops in a downward direction is known as the free jet region. The stagnation zone is the point where the jet meets the horizontal bottom wall. The wall jet zone is the horizontal channel flow downstream of the stagnation zone. Figure 3 presents velocity contours and streamlines of the radial convergent channel at different height ratios and at Re = 5,000 on the r-z midplane. It shows that the jet impinges on the surface and then flows in a transverse direction close to the bottom wall. As the effective cross-sectional flow area increases, the fluid velocity decreases in the radial direction. Also, a flow recirculation zone occurs due to flow reversal along the radial direction. There are minor vortexes at the outflow channel. These vortexes exist because of the secondary jet at the outflow, and as the HR decreases, entertainment gets stronger. As shown, the converging annular channels affect the intensity and structure of the main flow recirculation. As the height ratio increases, the length of the flow recirculation zone increases. A smaller flow recirculation zone is advantageous leading to lower pressure drop penalties. This is shown in Figure 4 quantifying the length ratio of the recirculation zone versus the height ratio at Re = 5,000 and 25,000. A converging annular channel reduces the flow cross-sectional area and restricts the fluid flow in the radial direction, thereby effectively shrinking the recirculation zone. Figure 4 also indicates that the length of the recirculation zone increases at higher flow rates due to augmented negative pressure gradients.

To gain further insight into the flow structure, Figure 5 presents the radial velocity profiles in the Z direction of all channel height ratios at different radii at Re = 5,000. At $r = 4$ and 8 mm, the flow reversal and, thus, the recirculation zone are present at all channel height ratios. However, both the strength and the extent of the recirculation zone decrease at lower channel height ratios as the radius increases from 4 to 8 mm. At $r = 11$ mm, the recirculation zone disappears at channel height ratios of 0.25 and 0.5, and radial velocity has only positive values in the radial direction. At $r = 15$ mm, the recirculation zone is absent for all channel height ratios. Additionally, at small radii, the magnitude of the flow velocity close to the heated wall is higher at higher height ratios. This is because, at small radii, the vertical extent of the circulation zone is higher at higher height ratios. Conversely, at large radii, the magnitude of the flow velocity close to the heated wall is higher at lower height ratios. This is because, at large radii, the effective flow cross-sectional area is smaller, resulting in higher flow velocities at lower height ratios.

Figure 6 shows turbulent kinetic energy (TKE) for HR = 1 and HR = 0.25 at Re = 25,000 and Re = 5,000 on the r-z midplane. It shows that the maximum TKE is located

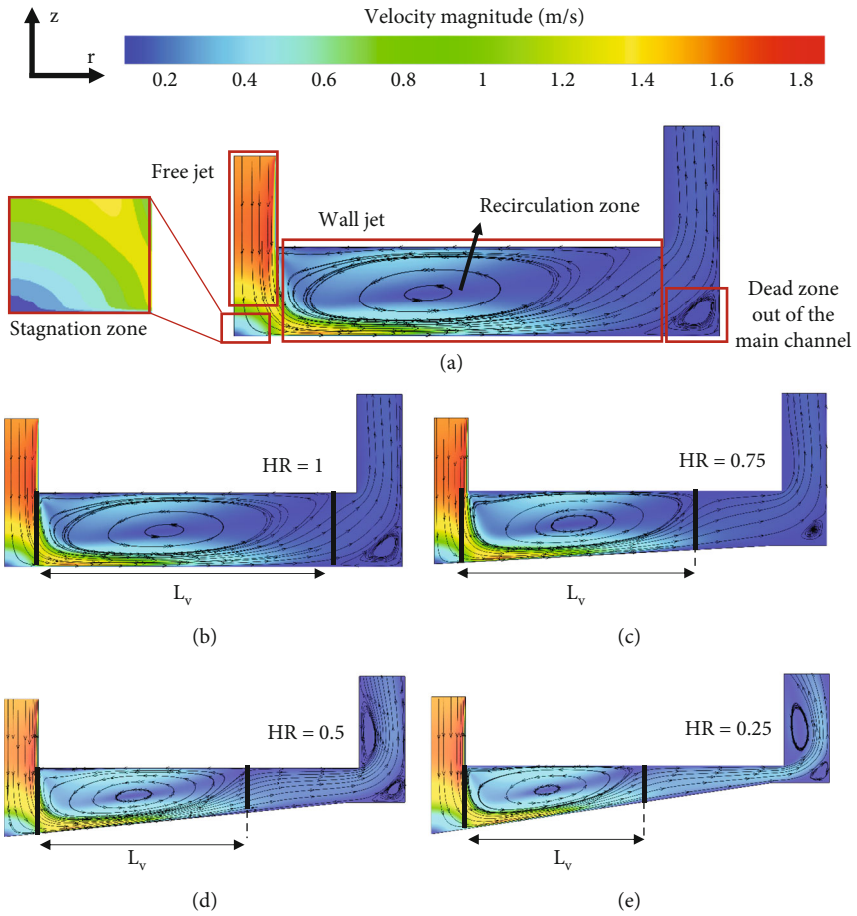

FIGURE 3: (a) Jet components in an annular jet impingement. Velocity contours and streamlines of converging annular channels at different HRs of (b) 1, (c) 0.75, (d) 0.5, and (e) 0.25.

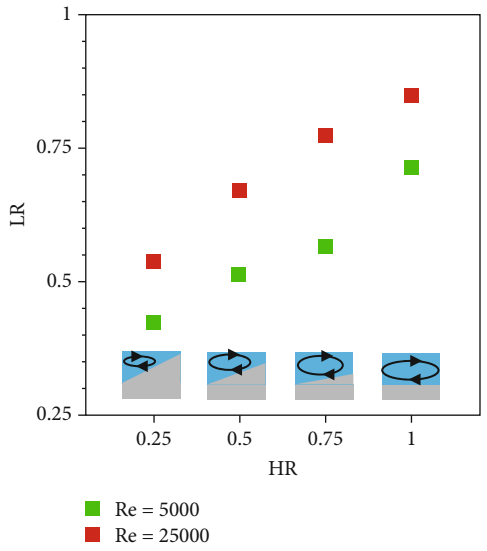

FIGURE 4: The recirculation length ratio versus channel height ratio at Re = 5,000 and 25,000.

beside the jet. This is because there is a stagnation zone at the center of the channel, and the maximum fluid velocity is at $r > R_j$. Also, Figure 6 demonstrates that TKE decreases in the radial direction due to the lower fluid velocity at large radii. Comparing TKE at Re = 5,000 and Re = 25,000, it shows that TKE is higher at Re = 25,000 due to the high fluid velocity and turbulent flow in the channel. Furthermore, it can be seen that the stagnation zone is larger at Re = 25,000 and TKE is high at the wall jet zone.

Figure 7(a) shows the pressure drop versus Re at different height ratios. As shown, at a given height ratio, the pressure drop increases with the Re number due to the augmented frictional losses at higher Re numbers. At a given Re number, the pressure drop penalty decreases as the height ratio decreases due to a reduced recirculation zone. For instance, the pressure drop is reduced by 59% when the height ratio reduces from 1 to 0.25 at Re = 25,000. Figure 7(b) shows the normalized pressure drop versus height ratio at Re = 5,000 and 25,000. As shown, the normalized pressure drop decreases at a higher rate at higher Re numbers as the height ratio decreases.

3.2. Effects of Converging Annular Channels on the Thermal Performance. The effect of converging channels on the flow

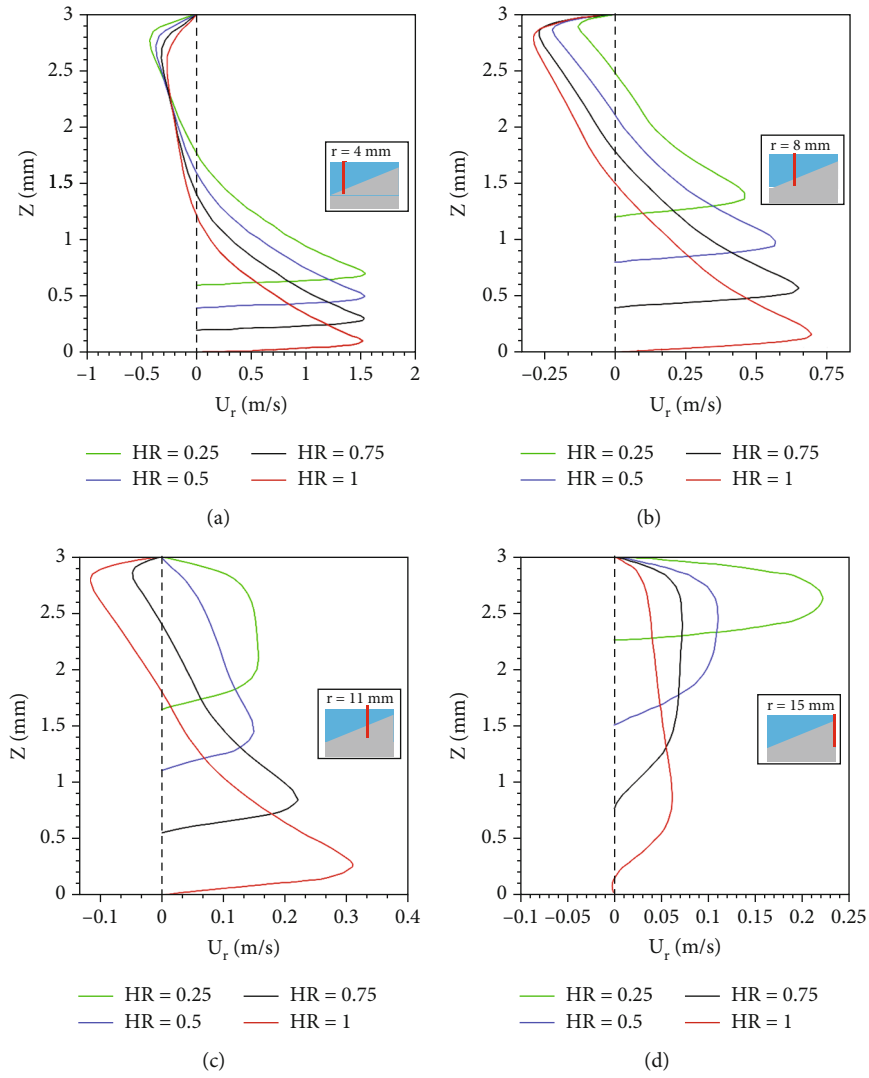

FIGURE 5: Radial flow velocity profiles in the Z direction of all channel height ratios at different radii of (a) 4 mm, (b) 8 mm, (c) 11 mm, and (d) 15 mm at Re = 5,000.

structure was discussed in the previous part. In this section, the effects of converging channels on thermal performance are investigated and justified. Figure 8 shows the local heat transfer coefficients versus radius for two height ratios of 0.25 and 1 at Re = 5,000. Defining the local heat transfer coefficient as $h_{\text{local}} = q''_r/(T_r - T_{f,\text{bulk}})$ and employing exact heat flux and fluid bulk temperature at each radial position, the local heat transfer coefficient trend is different from the previous studies [46, 47]. It shows that the local heat transfer coefficient is low at the center of the channel and its maximum value is around $r = 2$ mm. The location of these radii corresponds to the location of the maximum value of TKE in the radial direction. As shown, the local heat transfer coefficient decreases in the radial direction in both cases. This is attributed to the growth of the thermal boundary layer as well as the drop in the radial flow velocity in the radial flow direction. Also, TKE decreases in the radial direction, affecting heat transfer mechanisms. In the region of $4 < r < 11$ mm, the heat transfer coefficient is lower at HR = 0.25 compared with that of HR = 1. As the HR reduces, the velocity magnitude increases due to the decreased flow cross-sectional area. On the other hand, as discussed in Figure 5, the extent of the recirculation zone decreases as HR decreases, resulting in a lower velocity magnitude. As a result of these two effects, the velocity magnitude is smaller at HR = 0.25 compared to HR = 1, thereby making the heat transfer coefficient lower at HR = 0.25. On the other hand, in the region of $r > 11$ mm, the heat transfer coefficient is higher at HR = 0.25 compared with that of HR = 0.25. At large radii, the recirculation area disappears, and the effects of decreased flow cross-sectional area are dominant at HR = 0.25. Therefore, the velocity magnitude is higher close to the heated wall, resulting in a higher heat transfer coefficient at HR = 0.25.

Figure 9 shows the temperature profile in the radial direction for all HRs at Re = 5,000 and Re = 25,000. It is shown that the minimum base temperature is at the center of the jet, while it rises in the radial direction due to the reduced fluid velocity. HR = 1 has the minimum base temperature at the jet center compared to the other cases. This

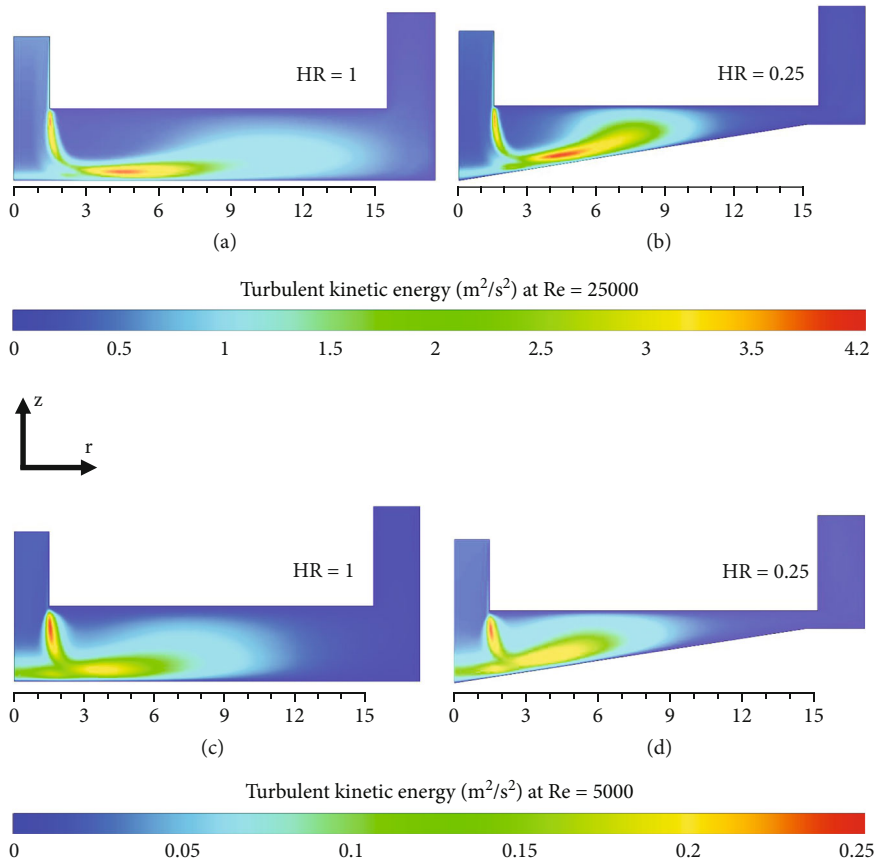

Figure 6: Turbulent kinetic energy for (a) HR = 1 and (b) HR = 0.25 at Re = 25,000 and (c) HR = 1 and (d) HR = 0.25 at Re = 5,000.

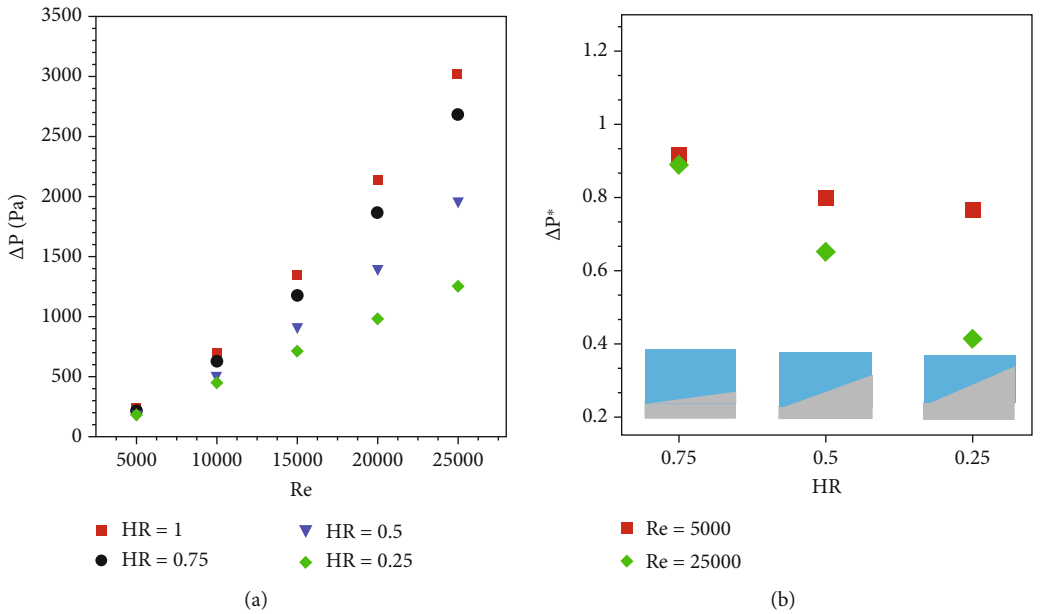

Figure 7: (a) Pressure drop versus Re number at different height ratios and (b) normalized pressure drop versus height ratio at Re = 5,000 and 25,000.

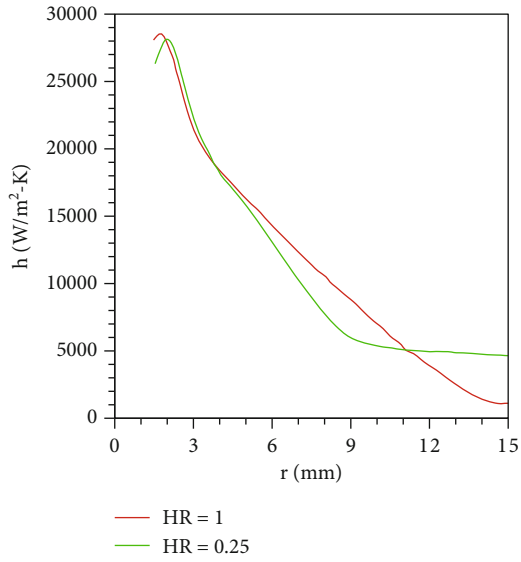

Figure 8: Local heat transfer coefficient versus radius at Re = 5,000.

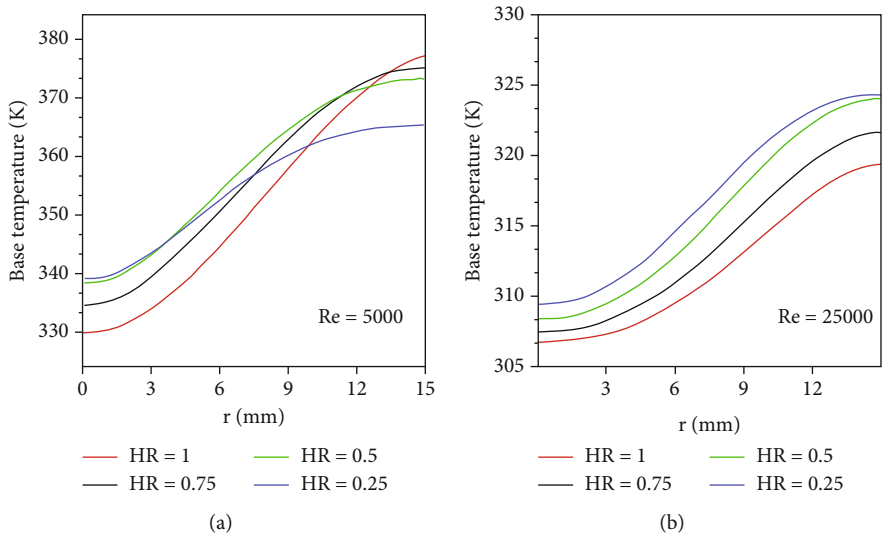

Figure 9: Temperature profiles in the radial direction for (a) Re = 5,000 and (b) Re = 25,000 for different HRs.

is because the stagnation zone expands as HR decreases [38]. Figure 9(a) shows that employing converging channels decreases the temperature at large radii. This is because velocity profiles change along the channel due to the different recirculation sizes, as discussed in Figures 4 and 5. However, HR = 1 has the lowest temperature values in the radial direction at Re = 25,000, as shown in Figure 9(b). This trend is different because extended recirculation area at higher Re number delays velocity profile change in the radial direction.

Figure 10(a) depicts the average heat transfer coefficient of the annular channels as a function of the Re numbers. At a given HR, the average heat transfer coefficient increases with the Re number due to a thinner thermal/velocity boundary layer. However, at a given Re number, the variation of the average heat transfer coefficient with HR depends on the value of Re. Figure 10(b) shows the normalized heat transfer coefficient for various height ratios at Re = 5,000 and Re = 25,000. It can be seen that a converging annular channel jet impingement heat sink has better thermal performance compared to the flat heat sink at low Re numbers. For instance, at Re = 5,000, the average heat transfer coefficient of HR = 0.25 is 12% higher than the flat heat sink. However, at high Re numbers, the flat heat sink has the best thermal performance. This different thermal behavior can be explained by considering the flow recirculation zone. At high Re numbers, the reduced heat transfer rate caused by the shrunk recirculation area of the converging channels dominates the increased heat transfer rate due to the decreased cross-sectional area of the converging channel when compared to the flat heat sink. Therefore, decreasing HR

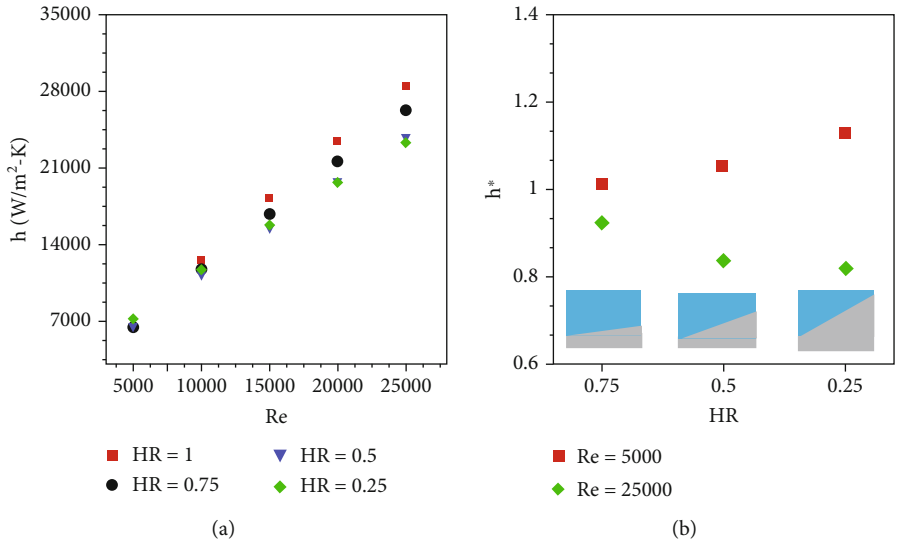

Figure 10: (a) Heat transfer coefficient for all the cases at different Re numbers and (b) normalized heat transfer coefficient for Re = 5,000 and Re = 25,000 at different HRs.

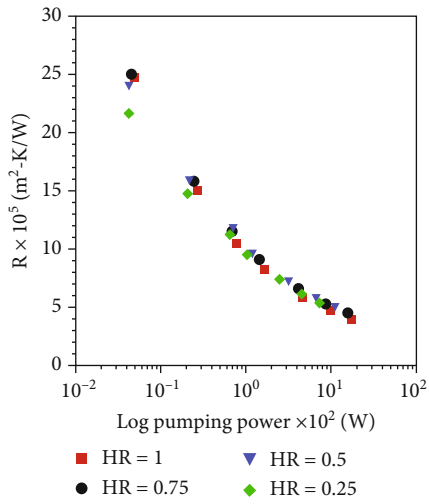

Figure 11: Thermal resistance versus pumping power.

deteriorates the average heat transfer coefficient at high Re numbers. For instance, at Re = 25,000, the average heat transfer coefficient of HR = 0.25 channel decreases by up to 19% compared to the HR = 1 flat heat sink.

3.3. Effects of Converging Annular Channels on the Overall Performance. As mentioned, the thermal performance of converging channels with low HRs degrades at high Re numbers. Considering both thermal and hydrodynamic performances, the thermal resistance as a function of the pumping power in all the cases is depicted in Figure 11. At low pumping powers, the converging channel with an HR of 0.25 has the minimum thermal resistance. However, at high pumping powers, there is no significant deviation between different cases. This is because, at high pumping powers, the reduced thermal resistance is balanced out with the increased pressure drop penalty. The data shows that a converging channel with an HR of 0.25 works best at low pumping powers and has a performance similar to a converging channel with an HR of 1 at high pumping powers.

4. Conclusions

This study investigated jet impingement in heat sinks with converging annular channels. The effects of channel height ratio and Re number on the hydraulic and thermal characteristics were investigated. It shows that although the vortex because of the entrainment does not have much effects on the thermal performance, recirculation size changes thermal behavior of the heat sink at small scales. The main outputs of this research are as follows:

(i) A converging annular channel improves the hydraulic performance of a jet impingement heat sink as it reduces the size of the recirculation area. At high Re numbers, the reduced pressure drop penalty is more considerable. For instance, at Re = 25,000, a jet impingement heat sink employing a converging annular wall with a height ratio of 0.25 showed a 59% lower pressure drop compared to a jet impingement heat sink with flat walls

(ii) It was found that the size of the recirculation zone affects thermal performance as well. A jet impingement heat sink employing a converging annular channel enhances the heat transfer coefficient at low Re numbers (12%), while it deteriorates the thermal performance at high Re numbers (17%) compared with the plain heat sink. At high Re numbers, the recirculation region shrinks, which reduces the heat transfer rate of a converging wall jet impingement heat sink compared with a flat wall jet impingement heat sink

(iii) At low pumping powers, a jet impingement heat sink employing a converging annular channel with a lower height ratio demonstrates better thermal and hydraulic performance. At high pumping powers, there is no obvious difference between jet impingement heat sinks with different height ratios

The outcomes of this research show that employing a convergent channel on a small scale changed the size of the recirculation area and the thermohydraulic characteristics of the channel. As the recirculation size can have a direct impact on the system, effective designs and optimizations can be developed for modifying this recirculation in a small scale. Additionally, conducting further research on the impacts of geometrical parameters would contribute to the advancement of understanding recirculation and its impact on the development of future jet impingement heat sinks that incorporate micro and porous structures, among other characteristics.

Nomenclature

D: Diameter (mm)
h: Heat transfer coefficient ($W \cdot m^{-2} \cdot k\text{-}1$)
H: Height (mm)
HR: Height ratio
K_e: Turbulent kinetic energy
k: Thermal conductivity ($W \cdot m^{-1}$)
L: Length (mm)
Nu: Nusselt
ΔP: Pressure drop (pa)
q'': Heat flux ($W \cdot m^{-2}$)
r: Radial direction
R: Radius (mm)
Re: Reynolds number
t: Thickness (mm)
T: Temperature (°C)
TKE: Turbulent kinetic energy ($m^2 \cdot s^{-2}$)
ΔT: Temperature difference (°C)
U: Velocity (m/s)
w: Outlet width (mm)
Z: Axial coordination.

Greek

ε: Turbulence dissipation
ρ: Density ($kg \cdot m^{-3}$)
μ: Dynamic viscosity ($kg \cdot m^{-1} \cdot s^{-1}$)
ϑ: Kinematic viscosity ($m^2 \cdot s^{-1}$).

Subscripts

ave: Averaged on surface
b: Solid base
c: Converging wall
e: Kinetic energy
f: Fluid
J: Jet inlet
r: Related to radial direction
s: Solid
v: Vortex
w: Related to wall
z: Related to axial direction
0: Base simulations for flat heat sink.

Data Availability

The datasets used and/or analyzed during the current study are available from the corresponding author on reasonable request.

Conflicts of Interest

The authors declare that they have no conflicts of interest.

Acknowledgments

This work is based upon research funded by Iran National Science Foundation (INSF) under project no. 4005020.

References

[1] Y. Li, M. Bai, Z. Zhou et al., "Numerical simulations for lithium-ion battery pack cooled by different minichannel cold plate arrangements," *International Journal of Energy Research*, vol. 2023, Article ID 8207527, 18 pages, 2023.

[2] C. Klinkhamer, S. Abishek, K. L. V. Iyer, R. Balachandar, and R. Barron, "Characterization of a jet impingement heat sink for power electronics cooling," *Thermal Science and Engineering Progress*, vol. 34, article 101408, 2022.

[3] G. AlFalah, T. S. Maatallah, and F. G. al-Amri, "Performance analysis of a singlecell-ultra-highconcentration photovoltaic thermal module based on pin-fins cooling microchannel," *International Journal of Energy Research*, vol. 46, no. 3, pp. 2947–2969, 2022.

[4] A. Rezazad Bari, M. Zabetian Targhi, and M. M. Heyhat, "A numerical study on thermo-hydraulic performance of micro pin-fin heat sink using hybrid pin-fins arrangement for electronic cooling devices," *International Journal of Numerical Methods for Heat & Fluid Flow*, vol. 33, no. 7, pp. 2478–2508, 2023.

[5] Q. Zhu, K. Chang, J. Chen et al., "Characteristics of heat transfer and fluid flow in microchannel heat sinks with rectangular grooves and different shaped ribs," *Alexandria Engineering Journal*, vol. 59, no. 6, pp. 4593–4609, 2020.

[6] M. Fathi, M. M. Heyhat, M. Zabetian Targhi, and S. Bigham, "Bifurcated divergent microchannel heat sinks for enhanced micro-electronic cooling," *International Communications in Heat and Mass Transfer*, vol. 146, article 106868, 2023.

[7] M. Fathi, M. M. Heyhat, M. Zabetian Targhi, and S. Bigham, "Porous-fin microchannel heat sinks for future microelectronics cooling," *International Journal of Heat and Mass Transfer*, vol. 202, article 123662, 2023.

[8] M. Ahmadi and S. Bigham, "Gradient wick channels for enhanced flow boiling HTC and delayed CHF," *International Journal of Heat and Mass Transfer*, vol. 167, article 120764, 2021.

[9] L. Hussain, M. M. Khan, M. Masud et al., "Heat transfer augmentation through different jet impingement techniques: a state-of-the-art review," *Energies*, vol. 14, no. 20, p. 6458, 2021.

[10] M. Fathi and A. Nejat, "Conjugate heat transfer investigation of impingement cooling for ribbed internal passage of a turbine vane," *International Journal of Thermal Sciences*, vol. 178, article 107589, 2022.

[11] S. Murugan, R. F. Huang, and C. M. Hsu, "Effect of annular flow pulsation on flow and mixing characteristics of double concentric jets at low central jet Reynolds number," *International Journal of Mechanical Sciences*, vol. 186, article 105907, 2020.

[12] Y. S. Bisht, S. D. Pandey, and S. Chamoli, "Experimental investigation on jet impingement heat transfer analysis in a channel flow embedded with V-shaped patterned surface," *Energy Sources, Part A: Recovery, Utilization, and Environmental Effects*, vol. 45, no. 4, pp. 12520–12534, 2023.

[13] A. Sarkar and R. P. Singh, "Air impingement technology for food processing: visualization studies," *LWT - Food Science and Technology*, vol. 37, no. 8, pp. 873–879, 2004.

[14] D. Qiu, C. Wang, L. Luo, S. Wang, Z. Zhao, and Z. Wang, "On heat transfer and flow characteristics of jets impinging onto a concave surface with varying jet arrangements," *Journal of Thermal Analysis and Calorimetry*, vol. 141, no. 1, pp. 57–68, 2020.

[15] A. Hadipour, M. Rajabi Zargarabadi, and M. Dehghan, "Effect of micro-pin characteristics on flow and heat transfer by a circular jet impinging to the flat surface," *Journal of Thermal Analysis and Calorimetry*, vol. 140, no. 3, pp. 943–951, 2020.

[16] N. G. Patil and T. K. Hotta, "A review on cooling of discrete heated modules using liquid jet impingement," *Frontiers in Heat and Mass Transfer*, vol. 11, 2018.

[17] S. V. Garimella, "Heat transfer and flow fields in confined jet impingement," *Annual Review of Heat Transfer*, vol. 11, no. 11, pp. 413–494, 2000.

[18] Z. H. Lin, Y. J. Chou, and Y. H. Hung, "Heat transfer behaviors of a confined slot jet impingement," *International Journal of Heat and Mass Transfer*, vol. 40, no. 5, pp. 1095–1107, 1997.

[19] H. C. Cui, J. H. Xie, R. Z. Zhao, M. Z. Wang, Z. C. Liu, and W. Liu, "Thermal-hydraulic performance analysis of a hybrid micro pin–fin, jet impingement heat sink with non-uniform heat flow," *Applied Thermal Engineering*, vol. 208, article 118201, 2022.

[20] Y. S. Bisht, S. D. Pandey, and S. Chamoli, "Jet impingement technique for heat transfer enhancement: discovering future research trends," *Energy Sources, Part A: Recovery, Utilization, and Environmental Effects*, vol. 45, no. 3, pp. 8183–8202, 2023.

[21] J. A. Fitzgerald and S. V. Garimella, "Visualization of the flow field in a confined and submerged impinging jet," *American Society of Mechanical Engineers, Heat Transfer Division*, vol. 346, pp. 93–96, 1997.

[22] V. Radmard, Y. Hadad, S. Rangarajan et al., "Multi-objective optimization of a chip-attached micro pin fin liquid cooling system," *Applied Thermal Engineering*, vol. 195, article 117187, 2021.

[23] S. Ndao, H. J. Lee, Y. Peles, and M. K. Jensen, "Heat transfer enhancement from micro pin fins subjected to an impinging jet," *International Journal of Heat and Mass Transfer*, vol. 55, no. 1-3, pp. 413–421, 2012.

[24] H. C. Cui, X. T. Lai, J. F. Wu, M. Z. Wang, W. Liu, and Z. C. Liu, "Overall numerical simulation and experimental study of a hybrid oblique-rib and submerged jet impingement/microchannel heat sink," *International Journal of Heat and Mass Transfer*, vol. 167, article 120839, 2021.

[25] T. Ming, C. Cai, W. Yang, W. Shen, and T. Gan, "Optimization of dimples in microchannel heat sink with impinging jets — part a: mathematical model and the influence of dimple radius," *Journal of Thermal Science*, vol. 27, no. 3, pp. 195–202, 2018.

[26] M. M. Keshtiban, M. Z. Targi, and M. M. Heyhat, "Combination of porous layer and jet impingement in an annular heat sink," in *2023 8th International Conference on Technology and Energy Management (ICTEM)*, pp. 1–5, Mazandaran, Babol, Iran, Islamic Republic of, February 2023.

[27] A. M. Bayomy and Z. Saghir, "Thermal performance of finned aluminum heat sink filled with ERG aluminum foam: experimental and numerical approach," *International Journal of Energy Research*, vol. 44, no. 6, pp. 4411–4425, 2020.

[28] S. Wiriyasart and P. Naphon, "Liquid impingement cooling of cold plate heat sink with different fin configurations: high heat flux applications," *International Journal of Heat and Mass Transfer*, vol. 140, pp. 281–292, 2019.

[29] R. D. Sundaram, S. Madhavan, P. Singh, and S. V. Ekkad, "Enhanced fin-effectiveness of micro-scale concentric-shape roughened target surface subjected to array jet impingement," *International Journal of Heat and Mass Transfer*, vol. 173, article 121148, 2021.

[30] S. Ndao, Y. Peles, and M. K. Jensen, "Effects of pin fin shape and configuration on the single-phase heat transfer characteristics of jet impingement on micro pin fins," *International Journal of Heat and Mass Transfer*, vol. 70, pp. 856–863, 2014.

[31] R. J. Goldstein, K. A. Sobolik, and W. S. Seol, "Effect of entrainment on the heat transfer to a heated circular air jet impinging on a flat surface," *Journal of Heat Transfer*, vol. 112, no. 3, pp. 608–611, 1990.

[32] C. Nuntadusit, M. Wae-hayee, and N. Kaewchoothong, "Heat transfer enhancement on a surface of impinging jet by increasing entrainment using air-augmented duct," *International Journal of Heat and Mass Transfer*, vol. 127, pp. 751–767, 2018.

[33] T. Guo, M. J. Rau, P. P. Vlachos, and S. V. Garimella, "Axisymmetric wall jet development in confined jet impingement," *Physics of Fluids*, vol. 29, no. 2, 2017.

[34] J. A. Fitzgerald and S. V. Garimella, "A study of the flow field of a confined and submerged impinging jet," *International Journal of Heat and Mass Transfer*, vol. 41, no. 8-9, pp. 1025–1034, 1998.

[35] M. Khoshvaght-Aliabadi, S. Deldar, A. Salimi, and M. M. Rashidi, "Effects of cross-section geometry on performance of corrugated miniature heat sink: uniform, convergent, divergent, and hybrid cases," *International Communications in Heat and Mass Transfer*, vol. 127, article 105269, 2021.

[36] M. R. Hajmohammadi, M. Bahrami, and M. Ahmadian-Elmi, "Thermal performance improvement of microchannel heat sinks by utilizing variable cross-section microchannels filled with porous media," *International Communications in Heat and Mass Transfer*, vol. 126, article 105360, 2021.

[37] V. S. Duryodhan, A. Singh, S. G. Singh, and A. Agrawal, "Convective heat transfer in diverging and converging microchannels," *International Journal of Heat and Mass Transfer*, vol. 80, pp. 424–438, 2015.

[38] B. Yousefi-Lafouraki, A. Ramiar, and A. A. Ranjbar, "Laminar forced convection of a confined slot impinging jet in a converging channel," *International Journal of Thermal Sciences*, vol. 77, pp. 130–138, 2014.

[39] B. Yousefi-Lafouraki, M. Rajabi Zargarabadi, and B. Sunden, "Hydrothermal analysis of pulsed jet impinging on a flat

surface with different pin configurations," *SSRN Electronic Journal*, 2022.

[40] P. Singh, M. Zhang, S. Ahmed, K. R. Ramakrishnan, and S. Ekkad, "Effect of micro-roughness shapes on jet impingement heat transfer and fin-effectiveness," *International Journal of Heat and Mass Transfer*, vol. 132, pp. 80–95, 2019.

[41] N. Satish and K. Venkatasubbaiah, "Numerical investigations of turbulent multiple jet impingement on a heated square block in a confined channel," *Thermal Science and Engineering Progress*, vol. 14, article 100415, 2019.

[42] H. A. Warda, E. M. Wahba, A. B. Rashad, and A. A. Mahgoub, "Experimental and numerical investigation of axial single scroll integral pumping devices for dual mechanical seals," *Alexandria Engineering Journal*, vol. 57, no. 4, pp. 2719–2728, 2018.

[43] T.-H. Shih, W. W. Liou, A. Shabbir, Z. Yang, and J. Zhu, "A new $k - \epsilon$ eddy viscosity model for high Reynolds number turbulent flows," *Computers & Fluids*, vol. 24, no. 3, pp. 227–238, 1995.

[44] A. Fluent, "MAN-ANSYS Fluent user' s guide Releasde 15.0," *Knowledge Creation Diffusion Utilization*, 2013.

[45] Z. Tang, Q. Liu, H. Li, and X. Min, "Numerical simulation of heat transfer characteristics of jet impingement with a novel single cone heat sink," *Applied Thermal Engineering*, vol. 127, pp. 906–914, 2017.

[46] S. V. Garimella and B. Nenaydykh, "Nozzle-geometry effects in liquid jet impingement heat transfer," *International Journal of Heat and Mass Transfer*, vol. 39, no. 14, pp. 2915–2923, 1996.

[47] F. Afroz and M. A. R. Sharif, "Heat transfer due to turbulent annular impinging jet with a bullet extension at the end of the inner blockage rod," *Case Studies in Thermal Engineering*, vol. 29, article 101704, 2022.